Journal of Solid State Chemistry **166,** 311–319 (2002)
doi:10.1006/jssc.2002.9593

Synthesis and Crystal Structures of Li_2CuZrO_4 Polymorphs

Christian Dussarrat,* Glenn C. Mather,†,[1] Vincent Caignaert,‡ Bernadette Domengès,‡ James G. Fletcher,§ and Anthony R. West‖

*Institut de chimie de la matiere condensée de Bordeaux, Chateau Brivazac, Avenue du Dr. A. Schweitzer, 33608 Pessac, France; †Consejo Superior de Investigaciones Científicas, Instituto de Cerámica y Vidrio, Antigua Cta. de Valencia, km. 24,300, 28500 Arganda del Rey, Madrid, Spain ; ‡Laboratoire CRISMAT-ISMRA, 6 Boulevard du Maréchal Juin, 14050 Caen Cedex, France; §Department of Chemistry, University of Aberdeen, Meston Walk, Old Aberdeen, Aberdeen, AB24 3UE, Scotland, United Kingdom; ‖Department of Engineering Materials, University of Sheffield, Sir Robert Hadfield Building, Mappin Street, Sheffield, S1 3JD, United Kingdom

Received August 7, 2001; in revised form March 6, 2002; accepted March 22, 2002

Two polymorphs of Li_2CuZrO_4 have been synthesized and their structures characterized by X-ray, neutron and electron diffraction. Both have novel types of ordered rock salt structure. β-Li_2CuZrO_4 is tetragonal, $a = 4.165(1)$ Å, $c = 9.418(1)$ Å, I-4*m*2, $Z = 4$, $R_I = 5.9\%$; the four sets of octahedral sites contain Zr, Li and partially ordered Li/Cu (two sets). γ-Li_2CuZrO_4 is orthorhombic, $a = 9.383(1)$ Å, $b = 5.894(1)$ Å, $c = 5.862(1)$ Å, *Cccm*, $Z = 8$, $R_I = 6.3\%$: in this case, the four sets of octahedral cation sites are fully ordered. Both structures show Jahn–Teller cooperative elongation of CuO_6 octahedra. The transition from the low-temperature γ polymorph to the high-temperature β phase is first order as indicated by the presence of a transition enthalpy at an onset temperature of 1047°C on heating.

INTRODUCTION

The family of phases, Li_2MXO_4: M = Mg, Mn, Fe, Co, Zn; X = Zr, Hf, have a double rock salt superstructure similar to α-$LiFeO_2$, but with partial order of cations: Li occupies one set of octahedral sites but M and X are disordered over a second set (1, 2). The related phase, Li_2CuZrO_4 was indexed on a similar tetragonal unit cell (2) but had a larger c/a ratio, attributed to a structural distortion associated with the Jahn–Teller active Cu^{2+} ion. In addition, extra powder X-ray diffraction (XRD) lines were observed indicating supercell formation with possible ordering of Cu and Zr atoms. Comparison of XRD patterns of samples cooled from different temperatures suggested that Li_2CuZrO_4 is polymorphic (3). We recently summarized the crystal structures of β- and γ-Li_2CuZrO_4 in a review of cation-ordered rock salt superstructure oxides (4, 5). Here, a more comprehensive study of Li_2CuZrO_4 is reported, covering crystal structure determination of the two polymorphs by a combination of X-ray, neutron and electron diffraction.

The following labeling scheme for the various structures is used. The label α is used for α-$LiFeO_2$ (although some authors have labeled this as γ) and the isostructural Li_2MXO_4 phases. For the latter family, only one polymorph has been generally encountered so far; a high-temperature polymorph containing complete cation disorder is, however, possible, as indicated for M = Ni (2). Other ordered, low-temperature polymorphs are also possible, especially with Jahn–Teller active M ions such as Cu^{2+}. Both polymorphs of Li_2CuZrO_4 described here are ordered forms of the α structure; they are therefore labeled β and γ; the γ structure is the more ordered, low-temperature polymorph.

EXPERIMENTAL

Li_2CuZrO_4 was prepared by solid-state reaction of Li_2CO_3, ZrO_2 and CuO over the temperature range 700–1100°C. The reagents were mixed in an agate mortar and fired in a Pt boat at 700°C to decarbonate for a few hours. Final firing of the low-temperature, light-green colored polymorph, γ-Li_2CuZrO_4, was at 1100°C for 24 h in a flow of O_2 followed by furnace cooling in O_2. The high-temperature, olive-green β polymorph was prepared from the pre-reacted material by firing at 1100°C under an O_2 flow followed by quenching in water. A small amount of CuO impurity was detected by XRD in both polymorphs; Cu_2O and $LiCu_3O_3$ were also detected in the β polymorph. Phase identification and unit-cell parameter determination was carried out by XRD using a Philips Hägg-Guinier focusing camera and Stoe Stadip powder diffractometer (transmission geometry), both $CuK\alpha_1$ radiation. For

[1] To whom correspondence should be addressed. Fax: +34-9187005500. E-mail: mather@icv.csic.es.

0022-4596/02 $35.00

Rietveld refinement, X-ray powder diffraction (XRD) data were collected at room temperature with a Seifert 3000 powder diffractometer (Bragg-Brentano geometry; Cu$K\alpha_1$ radiation) over the range $10^\circ \leq 2\theta \leq 150^\circ$ with a collection time of approximately 27 h. A detector stepwidth of 0.02° was employed, but the β polymorph was also recorded with a varying stepwidth program: 10–65° (stepwidth 0.01°), 65–115° (0.02°) and 115–160° (0.04°). The γ polymorph was also studied by neutron diffraction (ND) at room temperature with the D1a diffractometer (ILL, Grenoble) using a wavelength of 1.911 Å. Theoretical powder patterns for possible structural models were generated with the Stoe software program THEO; calculated and experimental patterns were then compared and parameters of the model refined by the Rietveld method with neutron and/or X-ray data using the program FullProf (6).

For transmission electron microscopy (TEM), powders were gently crushed in an agate mortar and deposited on a holey carbon-coated copper grid. Diffraction patterns were collected both with a medium-resolution JEM 2010 instrument using a tilting–rotating specimen holder and a TOPCON 2B high-resolution microscope equipped with an objective lens with a spherical aberration constant of 0.8 mm and a point-to-point resolution of 0.18 nm.

Compositional analysis was carried out on β and γ polymorphs with a Cameca SX51 electron probe microanalyzer. Standards used were $ZrSiO_4$ (for Zr) and CuO (for Cu). The grain size of both samples was small and it was necessary to use the instrument in fixed beam rather than raster mode, thus placing greater uncertainty on the results of the analysis; oxygen was not determined directly, therefore. The EPMA results, Table 1, provide a check on the Cu:Zr ratio. The copper content of the β phase is slightly lower than expected; by EPMA, both samples contained a small amount of CuO as a second phase impurity. Differential thermal analysis (DTA) was carried out under a flow of oxygen on a Setaram Labsys instrument over the temperature range 25–1100°C with two heating-cooling rates of 5 and 10°min^{-1}.

TABLE 1
Electron Microprobe Compositional Analysis of Li_2CuZrO_4 Phases

	By EPMA	Expected
β-Li_2CuZrO_4		
Cu	10.0(1)	12.5
Zr	11.3(4)	12.5
γ-Li_2CuZrO_4		
Cu	11.7(3)	12.5
Zr	12.1(2)	12.5

Note. At% averaged over 8 points (β phase) and 10 points (γ phase); e.s.d.s in parentheses.

STRUCTURE DETERMINATION

γ-Li_2CuZrO_4

X-Ray and Neutron Diffraction

The powder diffraction pattern of γ-Li_2CuZrO_4 was indexed on a C-centered orthorhombic, pseudo-tetragonal cell with the approximate geometrical relationship to the simple cubic rock salt structure: $a_\gamma = 2a$, $b_\gamma \approx c\gamma = \sqrt{2}a$. Indexed XRD data collected with the Stoe Stadip diffractometer have been published in the ICDD (7).

Various trial models for the structure of γ-Li_2CuZrO_4 were tested in space groups *Cccm* (No. 66) and *Ccc*2 (No. 37), bearing in mind that the structure was likely to be rock-salt-related with cubic-close-packed (ccp) oxide ions and cations ordered, or partially ordered, over the available octahedral sites. Using space group *Ccc*2, the positional parameters associated with the *z*-coordinate of both oxygen positions and the *y*-coordinate of one oxygen, O(2), failed to converge. Refinement proceeded satisfactorily in space group *Cccm*, but the oxygen positional parameters are no longer variable.

At this stage, the profile *R*-factors were somewhat poorer than expected for a relatively simple structure; this is attributable to an anisotropic and inconsistent full-width at half-maximum (FWHM) distribution for the Bragg reflections, rather than to a structure determination which was only partially correct. On inspection of the rather limited number of powder reflections, there appeared to be no obvious correlation between the order of the reflection index and the peakwidth as occurs, for example, with strain and defect broadening. Several samples of γ-Li_2CuZrO_4 were made in two laboratories using alternative precursor materials but no changes were found in the XRD patterns. A sequence of annealing regimes at different temperatures was also employed to study the stability of the γ phase but, at each temperature, the X-ray reflection profiles were identical. These results provide strong evidence that the anomalous peak-profile shapes are an intrinsic feature of the thermodynamically stable γ phase. The only correlation found between sharp and broadened reflections is given by the cell–parameter relation existing between the low- and high-temperature polymorphs: the broadened reflections of the former are not allowed for the high-temperature polymorph (β-Li_2CuZrO_4), i.e., reflections with $k + l = 2n + 1$. Hence, for the Rietveld refinement of the XRD data, the (*hkl*) reflection set was split into two: one set with $k + l = 2n$ and another with $k + l = 2n + 1$. An empirical structural model was then constructed in which each reflection set adopted independent profile parameters. This model added only one Lorentzian parameter and was refined with the FullProf software. On refinement, the goodness-of-fit parameter (χ^2) is reduced significantly from 2.84 to1.96.

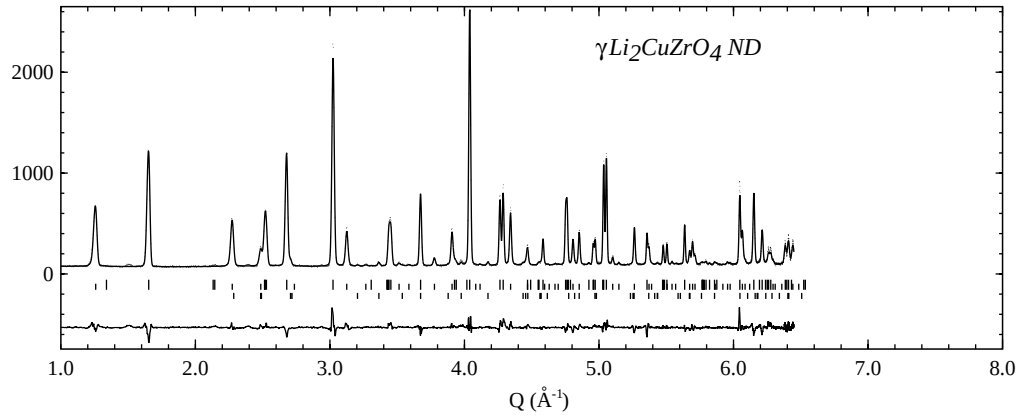

FIG. 1. Observed and difference neutron powder diffraction profiles of γ-Li_2CuZrO_4. Tick marks indicate the positions of reflections for γ-Li_2CuZrO_4 (top) and CuO (bottom); small tick marks are $k + l = 2n + 1$ reflections.

Due to the higher relative scattering factors of Li and O to neutrons compared to X-rays, neutron diffraction was carried out on the γ phase to characterize more accurately both the oxygen positions and the oxygen and lithium thermal vibration parameters. As a result of the larger instrumental profile of the D1A neutron beam, the peak-shape inconsistencies, which resulted in a poor X-ray fit, were largely masked in the neutron refinement. Taking the X-ray structure as a starting point for a combined X-ray–neutron refinement, it was found that the Li(1) thermal vibration parameter was very high (greater than 3.9 $Å^2$). A Fourier difference map indicated that the Li(1) position may be split. Li(1) was, thus, placed on the 8*e* site with an occupation of 0.5 and its positional parameters refined. This led to a decrease in χ^2 from 4.19 to 3.93 and the *B*-value refined to a more reasonable value of 1.7 $Å^2$. Despite the poorer resolution of the neutron data in comparison with the XRD data, the profile could be improved slightly using a model based on different reflection sets, as observed by electron diffraction and refined by XRD. The refinement was also better when the CuO second phase was included even though the amount of CuO impurity was <2 wt%. The observed and difference profiles of γ-Li_2CuZrO_4 are shown in Figs. 1 and 2 for ND and XRD data, respectively. Final atomic coordinates, bond lengths and bond valences are given in Table 2.

Electron Diffraction

Electron diffraction was employed to examine further the cause of the unusual XRD peak-profile shapes. Reciprocal space construction showed that the majority of crystallites consisted of domains oriented at 90° to one another corresponding to the interchange of **b**- and **c**-axis. This twinning along the (011) and (0−11) planes is not unexpected considering the similar magnitudes of the **b** and **c** cell parameters. The selected-area electron diffraction (SAED) patterns of Fig. 3 were taken under the same

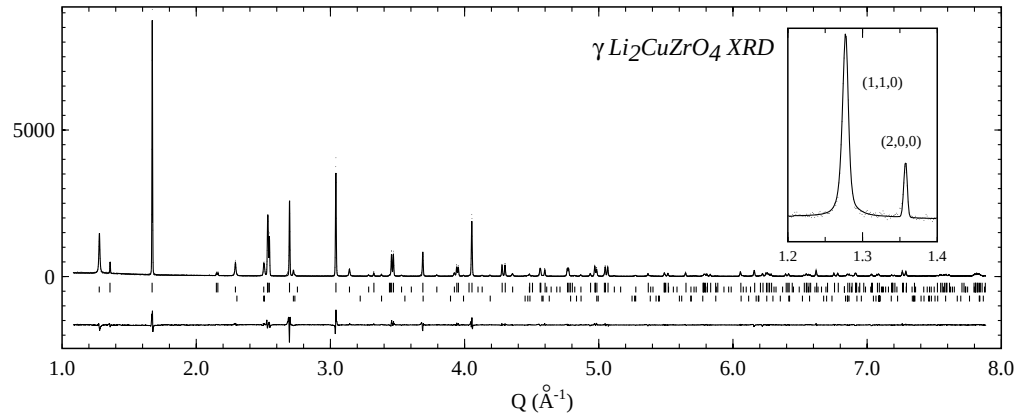

FIG. 2. Observed and difference X-ray powder diffraction profiles of γ-Li_2CuZrO_4. Tick marks indicate the positions of reflections for γ-Li_2CuZrO_4 (top) and CuO (bottom); small tick marks are $k + l = 2n + 1$ reflections. The inset shows anisotropic broadening of the (110) reflection with respect to the (200) reflection.

TABLE 2
Atomic Parameters and Bond Lengths for γ-Li_2CuZrO_4. Coupled XRD-ND Refinement

Cccm $a = 9.385(1)$ Å, $b = 5.895(1)$ Å, $c = 5.863(1)$ Å[a]						
Atom	Site	x	y	z	B_{iso}	Occupancy
Li(1)	8*l*	0.210(4)	0.742(10)	0	1.7(3)	0.5
Li(2)/Cu(2)	4*b*	0	$\frac{1}{2}$	$\frac{1}{4}$	0.5(3)	0.97/0.03(1)
Cu(3)/Li(3)	4*d*	0	0	$\frac{1}{4}$	0.58(6)	0.95/0.05(1)
Zr	4*e*	$\frac{1}{4}$	$\frac{1}{4}$	0	0.28(3)	1
O(1)	8*l*	−0.0246(7)	0.228(1)	$\frac{1}{2}$	0.43(6)	1
O(2)	8*g*	0.2662(7)	0	$\frac{1}{2}$	0.55(6)	1
		Distance to O(1) in Å			Distance to O(2) in Å	
Li(1)		2.20(4) (× 1)			2.06(4) (× 2)	
					2.18(4) (× 2)	
Li(2)		2.185(5) (× 4)			2.194(7) (× 2)	
Cu(3)		2.001(5) (× 4)			2.498(7) (× 2)	
Zr		2.119(6) (× 2)			2.0838(5) (× 4)	

[a] $R_{Nwp} = 7.9\%$, $R_{Xwp} = 12.9\%$, $\chi^2 = 3.2$ ($\chi^2_N = 3.9$, $\chi^2_X = 2.01$), $R_{I_N} = 4.9\%$, $R_{I_X} = 6.33\%$.

conditions. The selector aperture permitted the isolation of two domains within the same microcrystal (Figs. 3a and 3b) oriented at 90° with respect to one another. The corresponding high-resolution images (Fig. 4) exhibit substantial contrast modulations that are attributable to local (dis-)ordering. From the high-resolution observations, most crystals appear to be composed of crystallites whose diameter is as small as 15 nm.

Local order–disorder phenomena are also encountered in a number of SAED patterns that exhibit complex diffuse streaks, often parallel to the **a**-axis as, for example, in Fig. 5. A microdiffraction pattern projected along the [1 0 0] zone axis, Fig. 6a, indicates further order–disorder complexities. As the reflection conditions are hkl, $h + k = 2n$; $0kl$ (k $= 2$n), $l = 2n$, the $\mathbf{b}^*$- and $\mathbf{c}^*$-axis may be distinguished in the First-Order Laue Zone (FOLZ) wherever the reflection condition $1kl$, $k = 2n + 1$ is met. However, careful observation of the Zero-Order Laue Zone (ZOLZ) reveals the presence of diffuse spots along the $\mathbf{c}^*$-axis corresponding to forbidden reflections which indicate the loss of the *c*-glide mirror perpendicular to **a**. These spots also occur in the perpendicular direction (along $\mathbf{b}^*$) and, thus, provide further evidence of 90°-oriented domains. These forbidden reflections can also be seen in the corresponding SAED pattern (Fig. 6b) where the diffraction area is much larger (approximate diameter, 1 μm). Another type of diffuse reflection can be observed in Fig. 6b which may correspond to the intersection of diffuse streaks parallel to $\mathbf{a}^*$ and the Ewald sphere on the $(100)^*$ plane such that a local doubling of d_{011} takes place. This

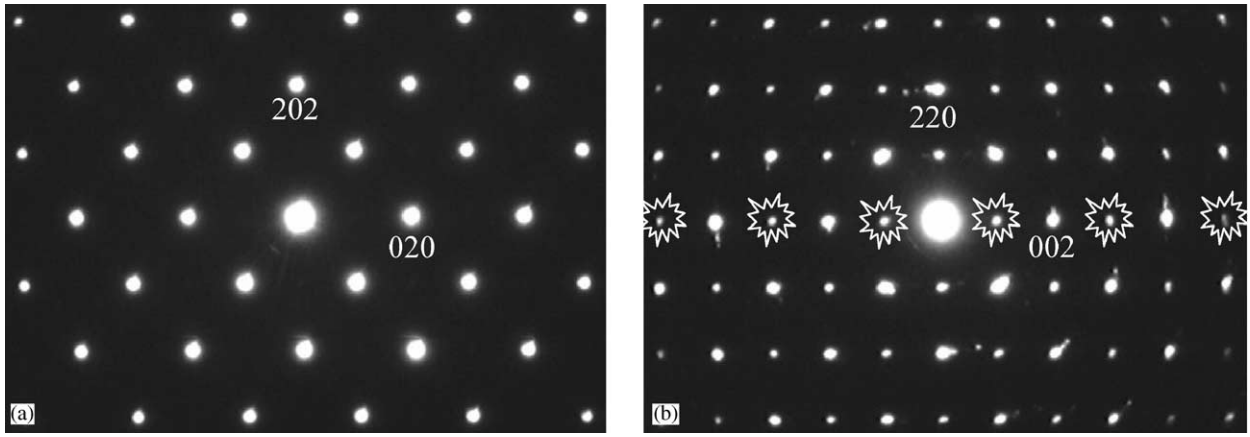

FIG. 3. SAED patterns of 90° rotated domains of a γ-Li_2CuZrO_4 microcrystal which can be indexed as follows: (a) [10–1] zone axis and (b) [1–10] zone axis; starred spots are due to double diffraction.

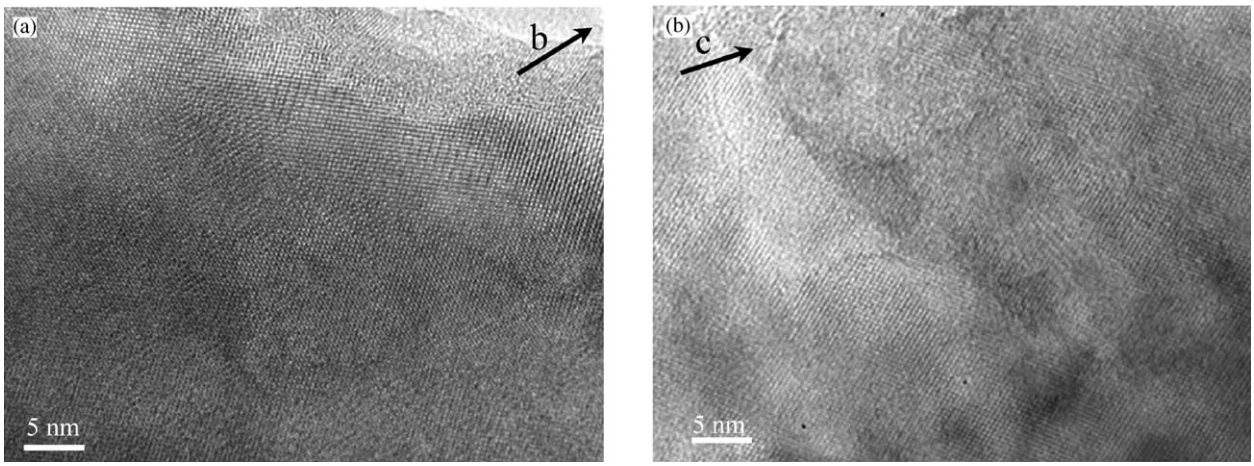

FIG. 4. High-resolution images of the same γ-Li_2CuZrO_4 microcrystal: (a) [10–1] zone axis and (b) [1–10] zone axis domain.

corresponds to the formation of a superstructure along [011] , i.e., the $\langle 100 \rangle$ rock-salt subcell direction, limited to small domains which are incoherent along **a**.

TEM thus points to the systematic twinning of crystals in the γ polymorph through exchange of **b**- and **c**-axis, although no planar domain boundary is observed; evidence of ordering is on only a very local scale and rotated domains are small. Complex diffusion observations provide further evidence of very local ordering phenomena. At the structural level, systematic rotation by 90° only affects the ordering in the Li–Cu rows since the chequered arrangement of the Zr is preserved from one domain to the other. As the Zr site (4*e*) has a special condition limiting possible reflections to $h, k, lk + l = 2n$, these reflections are not affected by the size of the domains, whereas the other reflections ($h, k, lk + l = 2n + 1$) are broadened. It is worth pointing out that the diffracting selected domains in electron diffraction is rather small compared to those in neutron and X-ray powder diffraction, thereby allowing the observation of local loss of symmetry related to the systematic 90° rotation of small domains which remains undetectable by the other techniques.

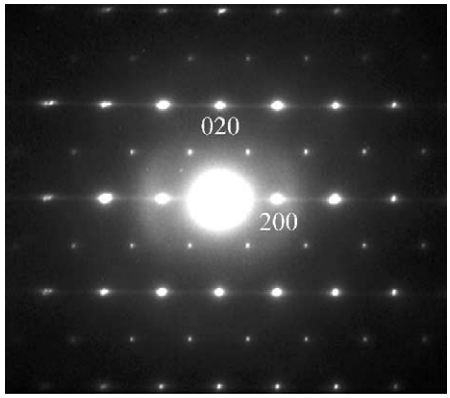

FIG. 5. SAED patterns projected along [0 0 1] showing diffuse streaks parallel to **a***.

β-Li_2CuZrO_4

XRD data were indexed on the tetragonal cell reported previously (1,7). Structural models were generated for β-Li_2CuZrO_4 with the Stoe software program THEO, as for the γ phase. A few space groups of type $I4^{***}$ were possible as no reflection conditions other than the body-centered lattice symmetry were observed. Similarities in unit-cell size and X-ray powder pattern had indicated that the structure was similar to Li_2MgZrO_4 but, in all probability, with a more complex cation order. Hence, various possible structural models with ccp oxide ions and similar cation ordering schemes to Li_2MgZrO_4 were tested. The structure was finally resolved in space group I-4m2 (or I4) and refined by the Rietveld method from its X-ray powder pattern.

In a model with the cation sites completely ordered and with one cation type per site, the Cu site had a particularly large B_{iso} value and one Li site refined to a negative value. It seemed, thus, that Cu and Li may share sites; a model with only partial order between one of the Li sites and Cu refined more successfully. The observed and difference XRD profiles of β-Li_2CuZrO_4 are shown in Fig. 7; atomic parameters and bond lengths are given in Table 3. As is the case for the γ polymorph, the profile parameters of the X-ray refinement show anisotropic broadening; the phenomenological model of anisotropic peak broadening proposed by Stephens (8) was, thus, used to describe the peak profiles. The values obtained for the degree of partial ordering between Li and Cu are approximate. Although ND may provide more information on the Li and Cu partial occupancies, we were unable to obtain β-Li_2CuZrO_4 in sufficient quantities to conduct this experiment because of its difficult synthesis.

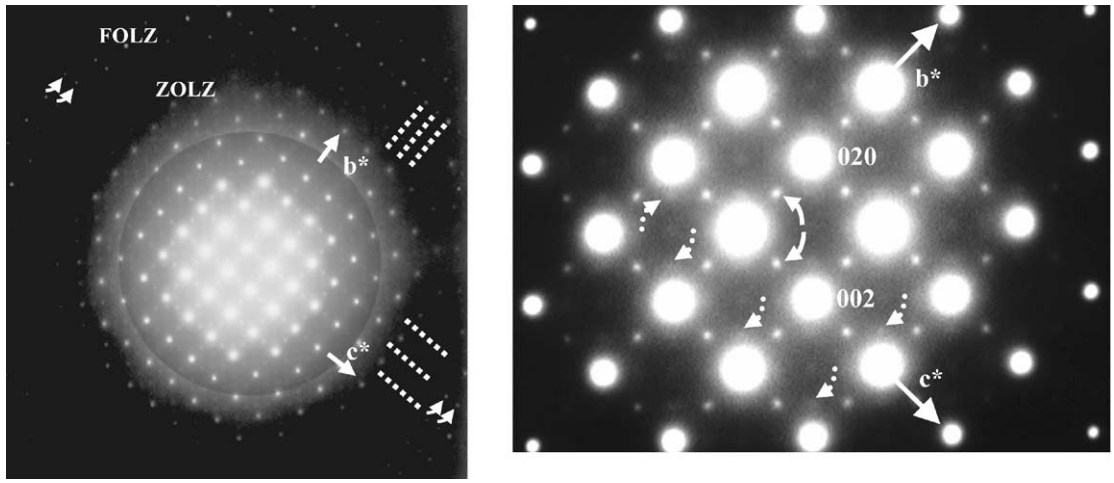

FIG. 6. Microdiffraction patterns projected along the [1 0 0] zone axis. FOLZ spots obey the condition: $1kl, k = 2n + 1$. On ZOLZ, forbidden reflections are indicated by plain curved arrows and diffuse extra reflections by dotted arrows.

Phase Transition

The phase transition from the γ- to the β-polymorph can be seen in the DTA thermogram, (Fig. 8). The temperature onset of endothermic and exothermic peaks is detected at 1053°C and 1037°C, respectively (heating and cooling rate $5°min^{-1}$). The extrapolation to a null heating rate led to a hysteresis of about 8°C between heating and cooling cycles, indicative of a first-order phase transition (inset of Fig. 8).

DISCUSSION

β-Li_2CuZrO_4 has a partially ordered rock salt superstructure with unique sites for Zr and one set of Li atoms and partial ordering of Cu and Li onto two separate sites. The unit cell and ion arrangement are shown in Fig. 9. There are four formula units per unit cell, with the relationship between supercell and rock salt subcell (RS), $s : a_\beta = a_{RS}, c_\beta = 2a_{RS}$. If we consider the structure to be composed of layers (but not close-packed layers) which stack along **c**, it can be seen that Zr and Cu order onto alternate layers, indicated by A and B, respectively. In the Zr-containing layers (A), Li (3) and Zr are fully ordered whereas the Cu-containing layers (B) are only partially ordered; for clarity, in Fig. 9 the Li and Cu positions in layer B are shown as fully ordered. Both Cu-containing sites show Jahn–Teller elongations of their octahedra. The only regular octahedra in the structure are, in fact, the ZrO_6 octahedra, as the $Li(3)O_6$ octahedra are also distorted. If we consider for the moment that the partially ordered Li/Cu sites are, instead, fully ordered, with Li fully occupying the Li/Cu(1) site and Cu fully occupying the Li/

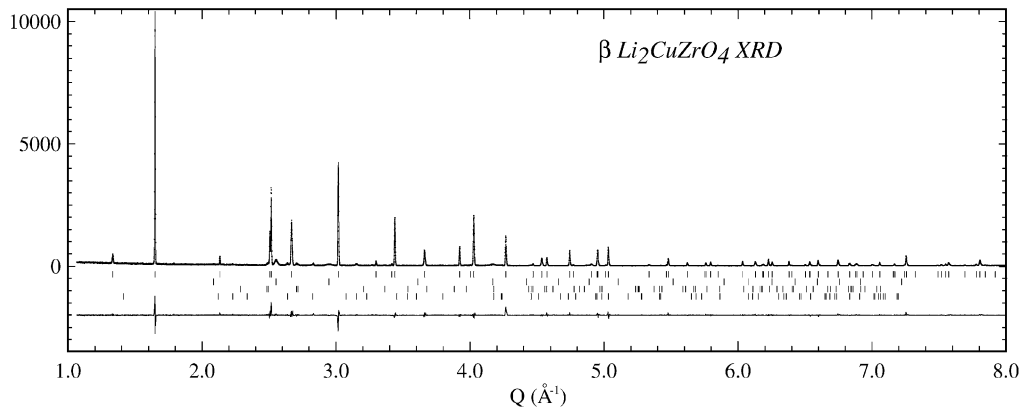

FIG. 7. Observed and difference X-ray powder diffraction profiles of β-Li_2CuZrO_4. Tick marks indicate the position of reflections for β-Li_2CuZrO_4, Cu_2O, CuO and $Li_3Cu_3O_3$ from top to bottom, respectively.

TABLE 3
Atomic Parameters and Bond Lengths for β-Li_2CuZrO_4. XRD Refinement

I-4*m*2 $a = 4.165(1)$ Å, c = 9.418(1) Å[a]						
Atom	Site	x	y	z	B_{iso}	Occupancy
Li(1)/Cu(1)	2*b*	0	0	$\frac{1}{2}$	0.49(8)[b]	0.78/0.22(2)
Cu(2)/Li(2)	2*a*	0	0	0	0.49(8)[b]	0.70/0.30(2)
Li(3)	2*d*	0	$\frac{1}{2}$	$\frac{3}{4}$	0.95[c]	1
Zr	2*c*	0	$\frac{1}{2}$	$\frac{1}{4}$	0.61(3)	1
O(1)	4*e*	0	0	0.24(1)	1.5(3)	1
O(2)	4*f*	0	$\frac{1}{2}$	0.473(4)	1.6(3)	1
		Distance to O(1) in Å			Distance to O(2) in Å	
Li(1)		2.45(11) (× 2)			2.098(5) (× 4)	
Cu(2)		2.26(11) (× 2)			2.098(5) (× 4)	
Li(3)		2.08(1) (× 4)			2.61(4) (× 2)	
Zr		2.084(5) (× 4)			2.10(4) (× 2)	

[a]Global weighted $\chi^2 = 2.92$, $R_I = 5.9\%$ (first scan), 8.3% (second scan), 17% (third scan).
[b]constrained to the same value.
[c]not refined.

Cu(2) site, then the structure would be an ordered polymorph of the Li_2MgZrO_4 (or α-$LiFeO_2$) structure; accordingly, the space group of β-Li_2CuZrO_4, *I*-4*m*2, is a subgroup of that of α-$LiFeO_2$, $I4_1/amd$.

The structure of γ-Li_2CuZrO_4 is a rock salt superstructure in which, unusually, complete cation order is achieved for three different cation types. There are very few examples of rock salt superstructures that display ordering among more than two different types of cation; one example is $Li_3Zn_2SbO_6$ (9). In γ-Li_2CuZrO_4 there are eight formula units per unit cell with the supercell:subcell relationship: $a_\gamma = 2a_{RS}$, $b_\gamma \approx c_\gamma \approx \sqrt{2}a_{RS}$. The cation arrangement and unit cells are shown in Fig. 10; again, oxygen positions have been omitted for clarity. Layers of ordered Li and Zr alternate with layers of ordered Li and Cu. The Li and Zr cations adopt a chequered arrangement within the Li/Zr layers, whereas within the Li/Cu layers, chains of edge-sharing CuO_6 octahedra and edge-sharing LiO_6 octahedra run parallel to each other and parallel to **c**. The CuO_6 octahedra show a considerable Jahn–Teller elongation, but the $Li(2)O_6$ octahedra within the Li/Cu layers are quite regular. The ZrO_6 octahedra are also relatively undistorted. The $Li(1)O_6$ octahedron is very

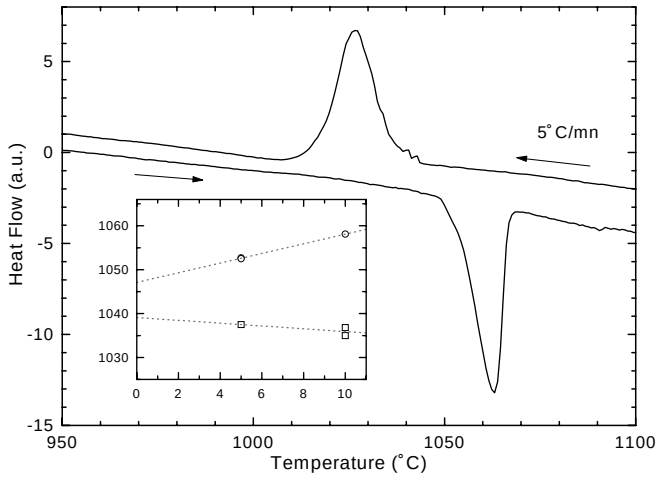

FIG. 8. DTA thermogram of Li_2CuZrO_4 at $5°C\,min^{-1}$. The inset shows T_{onset} for the endothermic (circle) and exothermic (square) peaks at two different heating rates ($5°C\,min^{-1}$ and $10°C\,min^{-1}$).

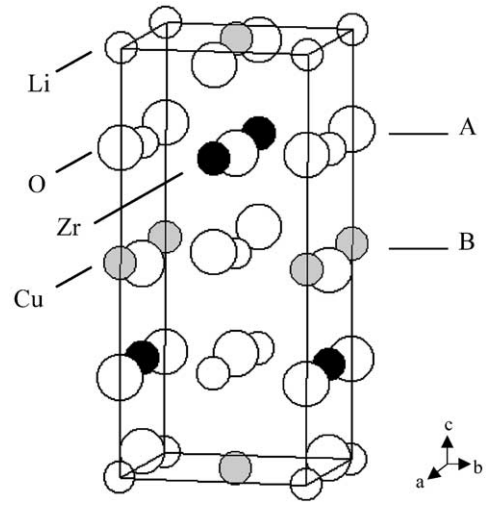

FIG. 9. Unit-cell and cation arrangement of β-Li_2CuZrO_4 showing Li/Zr-containing layers (A) and Li/Cu-containing layers (B) (A and B layers are not close packed). In the B layers, the order between Li and Cu is only partial but has been shown as complete for the sake of clarity.

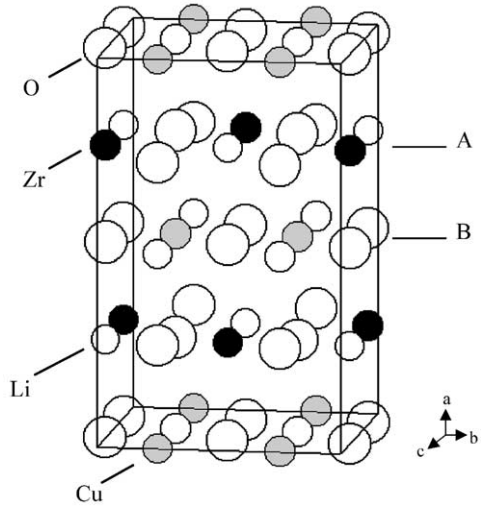

FIG. 10. Unit-cell and cation arrangement in γ-Li_2CuZrO_4 showing Li/Zr-containing layers (A) and Li/Cu-containing layers (B) (A and B layers are not closely packed).

elongated along **a** in a model in which this site is not split, but on splitting the site, the Li(1) coordination becomes five-fold and more regular.

The systematic twinning in the *bc* plane affects only the ordering in the Li–Cu rows. In fact, rotation of the structure through 90° can be conducted by translation while retaining the symmetry of the framework with the exception of these Li–Cu rows.

The bond valence concept (11, 12) can be used to give an indication of the correctness of the structure solution . The sum of the bond valences between a central atom, *i*, and neighboring atoms, *j*, should equal the valence, V_i, of atom *i*:

$$V_i = \sum_j b_{ij},$$

where b_{ij} is the bond valence determined from universal correlation curves which represent the bond valence–bond strength relationship for that bond in a number of structures. The bond valence values for each cation, calculated with parameters given in Ref. (13), are shown in Table 4; for mixed cation sites, the average bond valence has been calculated. For γ-Li_2CuZrO_4, all the calculated valence states are as expected, to be within $\sim$15%, and support the correctness of the structure solution. The discrepancies are, in general, somewhat larger for the β polymorph, particularly for the Li(3) site. However, in view of the empirical nature of bond valence calculations, the values are close enough to indicate that the β structure has also been correctly determined.

The driving force for ordering of Cu and Zr in Li_2CuZrO_4, as opposed to the statistical distribution of Zr and the divalent cation in the family α-Li_2MZrO_4: M = Mg, Mn, Fe, Co (1, 2), is almost certainly associated with the presence of Jahn–Teller active Cu^{2+} cations which results in an elongation of the *c*-axis by an extra 13% beyond that expected for a simple doubling of the rock salt cell. In other members of the Li_2MZrO_4 family, **c** is also greater than expected, but the effect is not so pronounced e.g., 5.5% in Li_2CoZrO_4. Copper ions order into alternate layers in both β and γ polymorphs so that the CuO_6 octahedra are adjacent and co-planar. This allows co-operative elongation of the Cu-containing octahedra leading to a tetragonal distortion of the unit cell. The phase transition from β to γ appears to occur when the energy gained by aligning the CuO_6 octahedra in edge-sharing chains (γ) becomes greater than the electrostatic repulsion energy associated with having Cu^{2+} cations in a *cis* configuration within an octahedral environment.

Li_2CuZrO_4 has an interesting analogue in the phase $NaMnO_2$ (14). This ordered rock salt also has two polymorphs. α-$NaMnO_2$ has the α-$NaFeO_2$-type structure, in which different cations separate into alternate layers between close-packed oxygens. β-$NaMnO_2$, however, has an ordered rock salt structure that is isostructural with $LiMnO_2$ (15). As in Li_2CuZrO_4, Pauling's rule is relaxed due to the presence of Jahn–Teller active cations and again, there are two types of cation environment around oxygen with nearest neighbors 4Na/2Mn and 2Na/4Mn, respectively. Adjacent MnO_6 octahedra edge-share and align themselves in chains parallel to chains of NaO_6 octahedra. The formation of a second polymorph with edge-sharing MnO_6 octahedra allows Jahn–Teller cooperative elongation of the MnO_6 octahedra.

CONCLUSIONS

Li_2CuZrO_4 is polymorphic, with β and γ rock-salt-related structures that differ in the manner in which the cations are ordered. In both structures, CuO_6 octahedra are aligned in layers, causing a Jahn–Teller elongation of

TABLE 4
Calculated Valence States in Li_2CuZrO_4 Polymorphs

Atom	Calculated valence state	Oxidation state
	β-Li_2CuZrO_4	
Li(1)	0.84	1
Li(2)/Cu(2)	1.02	1.22
Cu(3)/Li(3)	1.48	1.7
Zr	3.98	4
	γ-Li_2CuZrO_4	
Li(1)	0.85	1
Li(2)	0.86	1
Cu(3)	1.90	2
Zr	3.92	4

the unit cell. In β-Li_2CuZrO_4, the CuO_6 octahedra predominantly corner-share, whereas they edge-share in γ-Li_2CuZrO_4. TEM indicates that in the β polymorph systematic twinning of crystals takes place through exchange of the **b**- and **c**-axis. The phase transition from γ to β takes place at 1047°C and is first order as indicated by DTA.

ACKNOWLEDGMENTS

We thank A. M. Coats (University of Aberdeen) for the electron microprobe analyses, E. Suard (ILL) for the neutron diffraction data, and EPSRC for the financial support.

REFERENCES

1. M. Castellanos, A. R. West, and W. B. Reid, *Acta Crystallogr. C* **41,** 1707 (1985).
2. M. Castellanos, M. Chavez Martinez, and A. R. West, *Z. Krist.* **190,** 161 (1990).
3. B. Thiebaut, M.Sc. Thesis, University of Aberdeen, Scotland, 1994.
4. G. C. Mather, Ph.D. thesis, University of Aberdeen, Scotland, 1995.
5. G. C. Mather, C. Dussarrat, J. Etourneau, and A. R. West, *J. Mater. Chem.* **10,** 2219 (2000).
6. FullProf, J. Rodriguez-Carvajal, "Satellite Meeting on Powder Diffraction, Abstracts of the XVth Conference of the International Union of Crystallography," Toulouse, 127, 1990.
7. International Centre for Diffraction Data, Card No. 41–59.
8. P. W. Stephens, *J. Appl. Crystallogr.* **32,** 281 (1999).
9. C. Greaves and S. M. A. Katib, *Mater. Res. Bull.* **25,** 175 (1990).
10. G. Donnay and D. H. Donnay, *Acta Crystallogr. B* **29,** 1417 (1973).
11. I. D. Brown and R. D. Shanon, *Acta Crystallogr. A* **29,** 266 (1973).
12. I. D. Brown in "Structure and Bonding in Crystals," (M. O'Keeffe and A. Navrotsky, Eds.), 1st ed., Vol. 2, pp. 1–29. Academic Press, New York, 1981.
13. D. Altermatt and I. D. Brown, *Acta Crystallogr. B* **41,** 244 (1985); N. E. Breese and O'Keffe, *Acta Crystallogr. B* **47,** 192 (1991).
14. J. P. Parent, R. Olazcuaga, M. Devalette, C. Fouassier, and P. Hagenmuller, *J. Solid State Chem.* **3,** 1 (1971).
15. T. A. Hewston and B. L. Chamberland, *J. Phys. Chem. Solids* **48**(2), 97 (1987).